Stem Cell Reports, Volume *3*

Supplemental Information

Calcium Transients Closely Reflect Prolonged Action Potentials in iPSC Models of Inherited Cardiac Arrhythmia

C. Ian Spencer, Shiro Baba, Kenta Nakamura, Ethan A. Hua, Marie A.F. Sears, Chi-cheng Fu, Jianhua Zhang, Sadguna Balijepalli, Kiichiro Tomoda, Yohei Hayashi, Paweena Lizarraga, Julianne Wojciak, Melvin M. Scheinman, Katriina Aalto-Setälä, Jonathan C. Makielski, Craig T. January, Kevin E. Healy, Timothy J. Kamp, Shinya Yamanaka, and Bruce R. Conklin

Supplemental Fig. 1

1A

1B

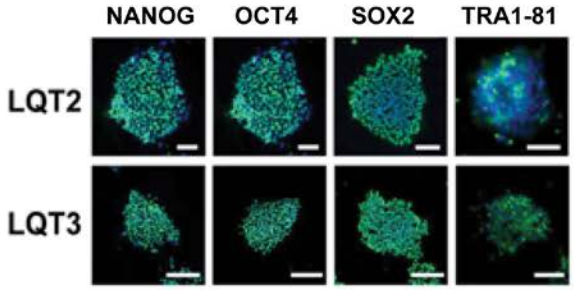

1C

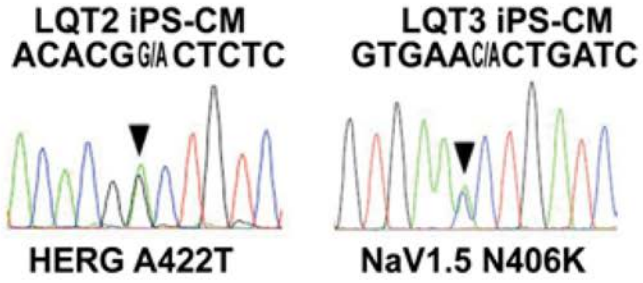

1D

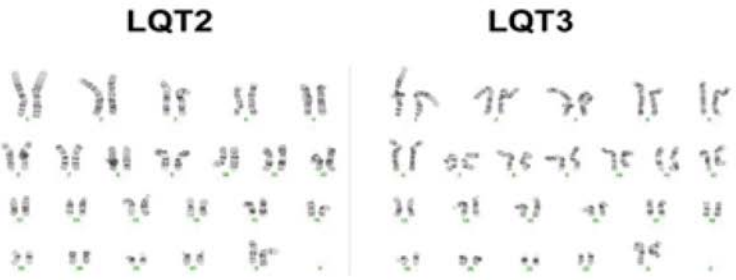

Figure S1. Generating iPS cell lines from LQT2 and LQT3 patients: related to production and differentiation of iPS cells in Experimental Procedures.

(A) Surface ECGs. LQT2 (upper) and LQT3 (lower) patients had a QT_c of 493 ms and 522 ms, respectively (normal upper limit = 480 ms).

(B) Immunocytochemistry of representative iPS colonies of undifferentiated LQT2 and LQT3 iPS cells transduced by retroviruses packaging OCT3/4, SOX2, KLF4, and c-MYC transcription factors. Transgene silencing was demonstrated by RT-PCR (not shown) and endogenous pluripotency markers NANOG, OCT4, SOX2, and TRA1-81 were well expressed in all cells in each colony as shown by GFP (green) staining. Nuclei were counterstained with Hoechst 33342 (blue). Scale bars: 50 μm.

(C) Heterozygous mutations, A422T (1264G>A) in the *KCNH2* gene and N406K (1218C>A) in *SCN5A*, detected in the genomic DNAs of LQT2 and LQT3 iPS cell lines. Lines: black, guanosine; green, adenosine; blue, cytidine; red, thymidine.

(D) Karyotypes of LQT2 and LQT3 iPS cells (analyzed commercially by Cell Line Genetics, Madison, Wisconsin, USA) were normal.

Supplemental Fig. 2

2A

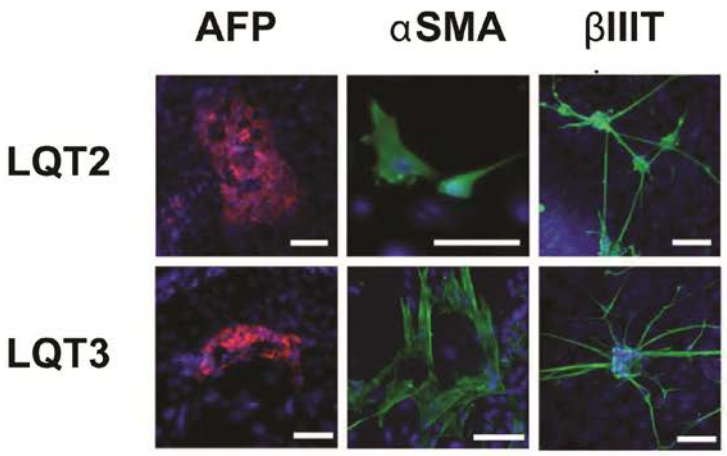

2B

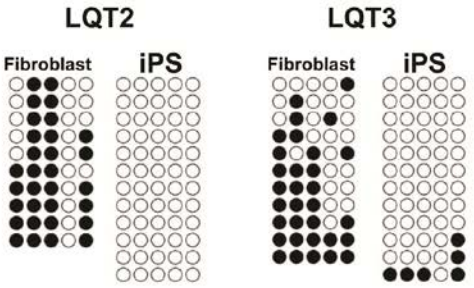

2C

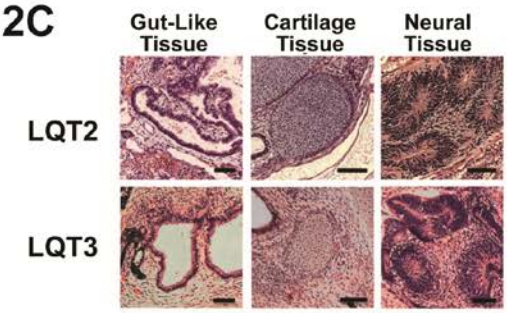

2D

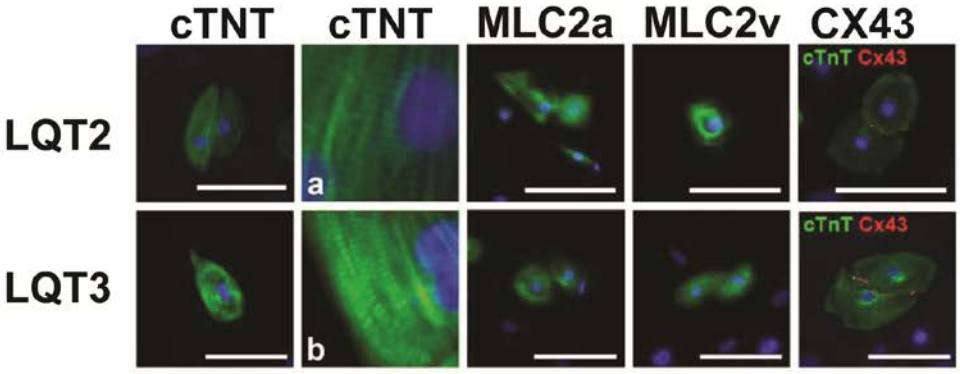

<u>Figure S2.</u> LQT2 and LQT3 iPS cells demonstrated pluripotency and directed differentiation to cardiomyocytes: related to production and differentiation of iPS cells in Experimental Procedures.

(A) Identification of all three embryonic germ layers after patient-derived iPS cells were differentiated in vitro by an embryoid body differentiation method. The germ layers were identified by immunocytochemistry: endoderm (AFP, alpha-fetoproteinpositive hepatocytes), mesoderm (α-SMA, smooth muscle actin–positive smooth muscle cells), and ectoderm (β-IIIT, beta tubulin–positive neurons). Nuclei were counterstained with Hoechst 33342 (blue). Scale bars, 10 μm.

(B) Bisulfite sequencing results showing that the OCT4 promoter is highly methylated (turned off) in original fibroblast lines, but unmethylated in iPS cell lines. Each circle represents a CpG sequence in the promoter region. Filled circles denote methylated CpG, and open circles show unmethylated CpG. These patterns are consistent with full reprogramming of iPS cells. (C) Teratomas also revealed that LQT2 and LQT3 iPS differentiated into all three germ layers in vivo: endoderm (gut-like tissues), mesoderm (cartilage tissue) and endoderm (neural tissues). Scale bars, 20 μm.

(D) Immunocytochemistry showed that after directed differentiation using the Matrix Sandwich Method (Zhang et al., 2012), LQT2 and LQT3 iPS cells differentiated into cTNT-, MLC2a-, and MLC2v-positive cardiomyocytes. CX43-positive gap junctions formed between cardiomyocytes. Nuclei were counterstained with Hoechst 33342 (blue). Scale bars, 10 μm.

Supplemental Fig. 3

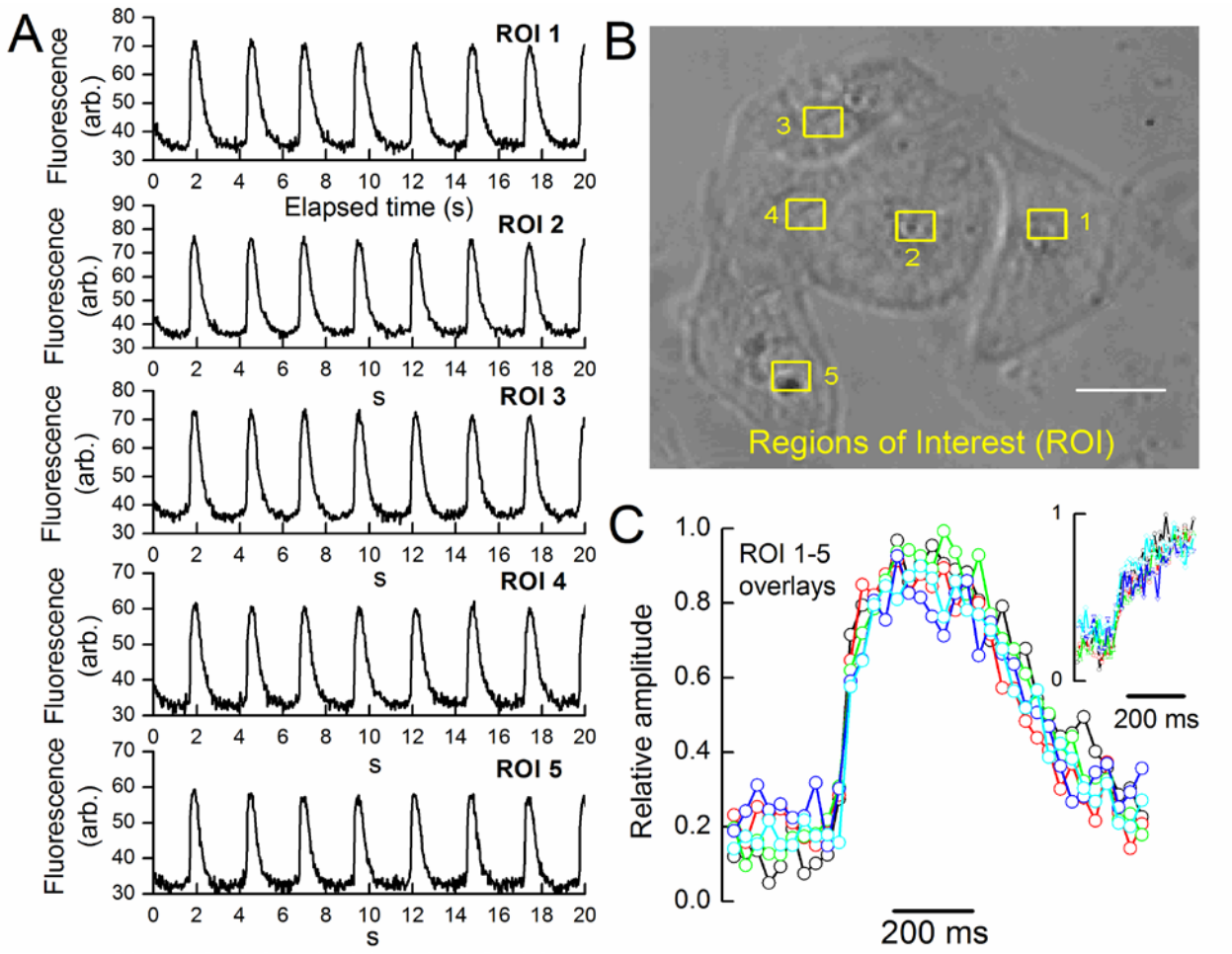

<u>Figure S3</u>. Comparing spontaneous $[Ca^{2+}]_i$ transients in individual myocytes of a control microcluster: related to *Functional Characterization of Control and LQT2 iPS-CM* in Results.

(A) Fluo-4 fluorescence was averaged in small regions of interest (ROI), such that each ROI was within a single myocyte of a five-cell microcluster and plotted (top to bottom) versus time (from videomicroscopy). The ROI number in the upper right corner relates to areas defined in ImageJ software.

(B) The numbered ROIs, within which fluorescence was averaged (yellow rectangles), are superimposed on a transmitted light image of the microcluster. Scale bar: 50 µm.

(C) Overlaid time-course plots for the same single spontaneous $[Ca^{2+}]_i$ transient measured in each ROI of the microcluster are shown at 30-ms resolution (33 frames/s in the videomicrograph). The rising phase of the transients superimpose completely within a single video frame. Inset: the equivalent $[Ca^{2+}]_i$ transient time courses were recorded at a resolution of 10 ms (100 frames/s). Despite a lower signal-to-noise ratio, the $[Ca^{2+}]_i$ transient upstrokes completely synchronized within a single video frame. Similar results were obtained from twenty microclusters recorded at 30-ms resolution and five microclusters at 10-ms resolution.

Supplemental Fig. 4

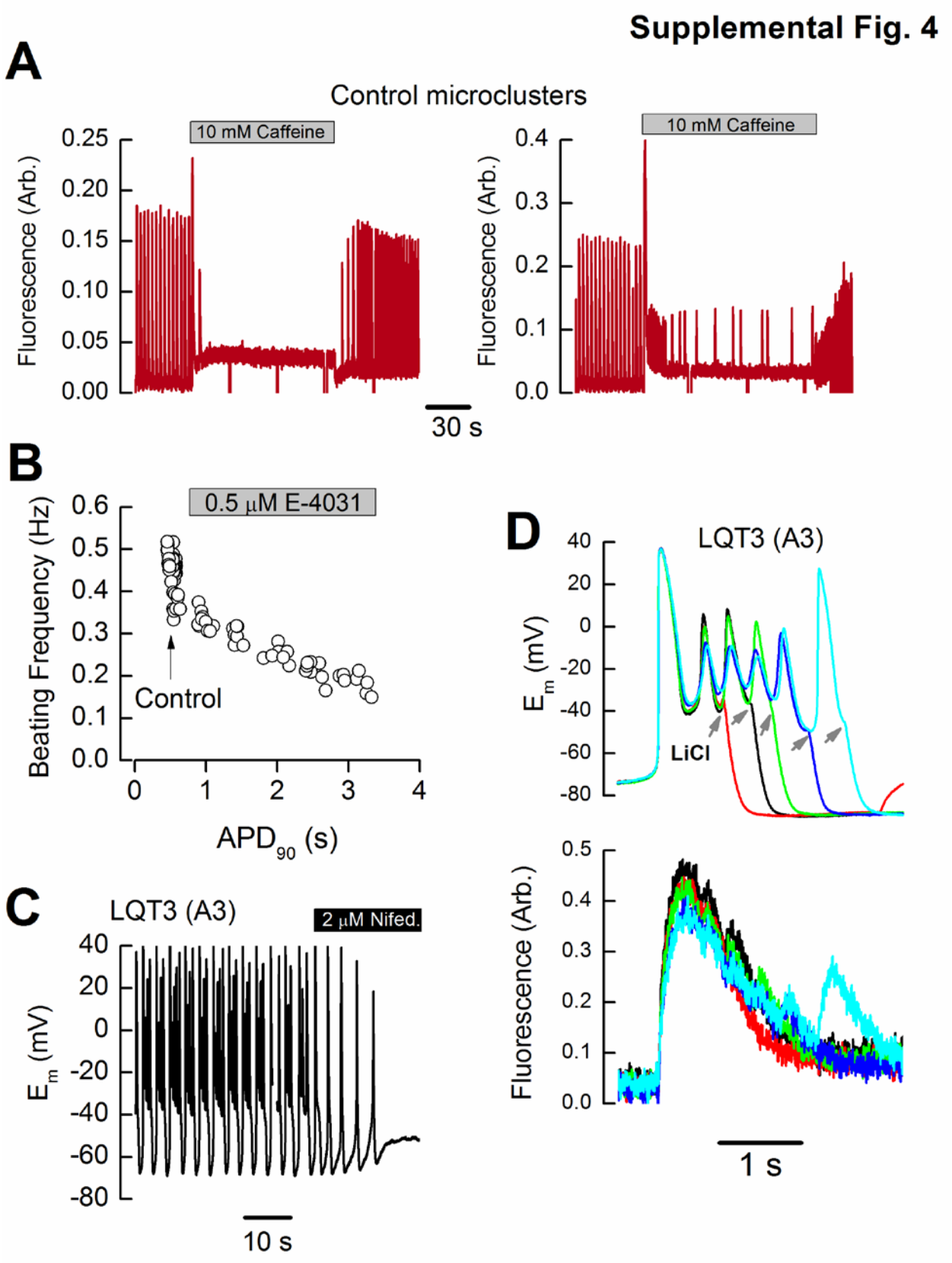

Figure S4. Additional pharmacology data: related to Results.

(A) Effects of superfusing 10 mM caffeine (gray bar) on spontaneous $[Ca^{2+}]_i$ transients (arbitrary units, red) recorded continuously in control microclusters. Caffeine initially evoked a large single $[Ca^{2+}]_i$ transient due to total release of the SR Ca^{2+} load, after which beating ceased in the majority (64%) of myocyte microclusters (left). Some microclusters continued to beat with $[Ca^{2+}]_i$ transients of reduced amplitude and frequency (right). Step-like downward deflections represent shutter closures. Timescale bar refers to both panels.

(B) Plot of beating frequency, calculated from each preceding diastolic interval, versus APD_{90} during E-4031 treatment of a control microcluster (shown in Figure 5). As I_{Kr} block increased, APs lengthened and the beating frequency fell in direct proportion.

(C) Effects of exposing a typical LQT3 (A3) microcluster to nifedipine (black bar). Blocking I_{Ca} caused dramatic AP abbreviation before beating ceased. During arrest, E_m was ≈–60 mV.

(D) Superimposed (color-coded) APs (E_m, Upper) and $[Ca^{2+}]_i$ transients (Lower, fluorescence in arbitrary units) from a representative LQT3 (A3) microcluster exposed to extracellular LiCl to block NCX after a sequentially increasing number of EADs (gray arrows). Each color represents the same AP and $[Ca^{2+}]_i$ transient, terminated by extracellular Li^+ at the time indicated by the arrow. Between Li^+ applications (traces), the microcluster was briefly permitted to return to steady-state beating.

Supplemental Fig. 5

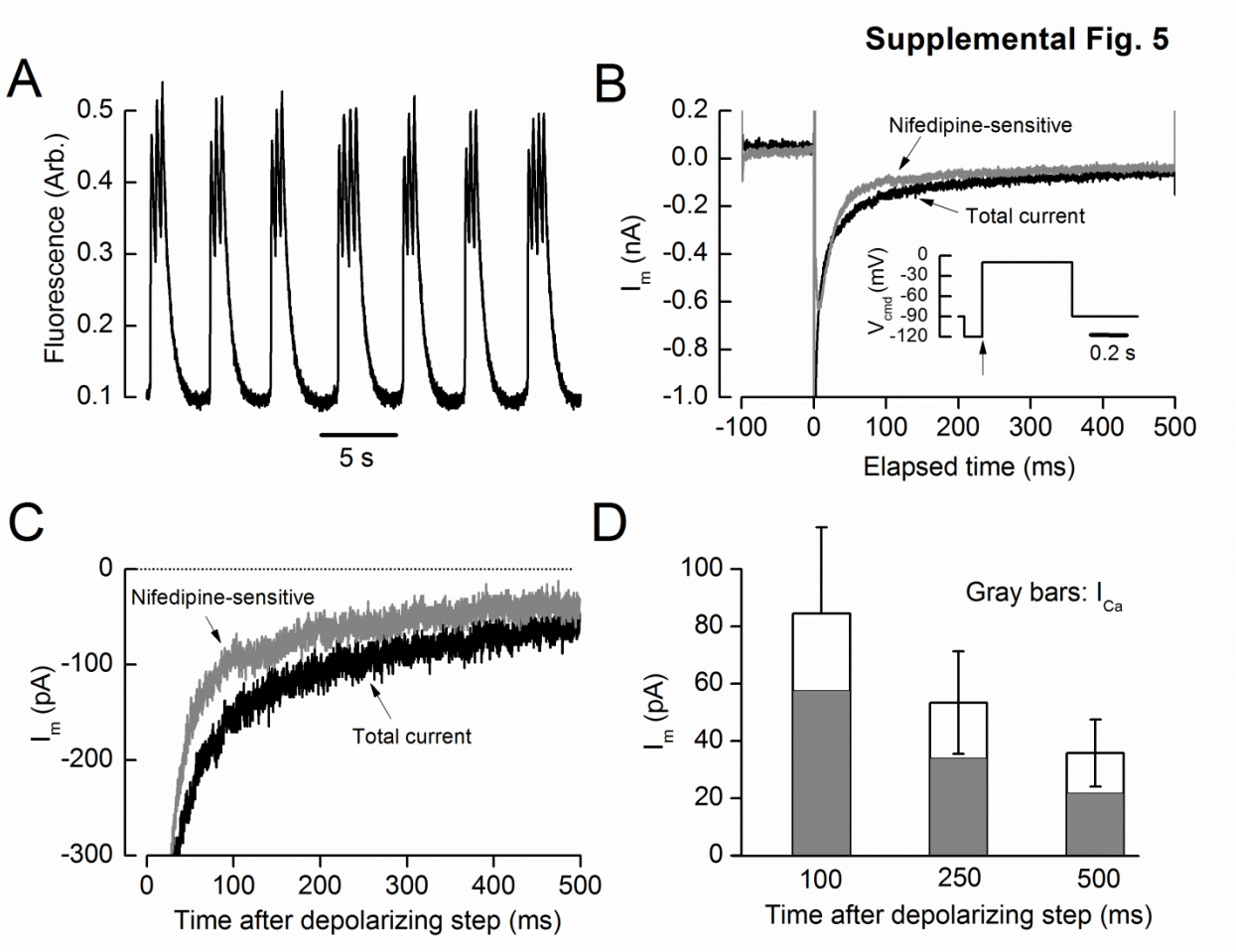

<u>Figure S5</u>. Late currents recorded in LQT3 (A1) iPSC-CM: related to Figure 6.

(A) Typical LQT3 Fluo-4 fluorescence transients (in arbitrary units) confirmed the usual prolongation phenotype before voltage-clamp (clone A1).

(B) Late currents were recorded in the same myocyte as (A) by applying the voltage command (V_{cmd}) shown in the inset (the arrow points to the step depolarization at time zero in the main figure). The time base was adjusted to make this point zero in subsequent panels. Plotted are the total current, sensitive to 50 µM TTX plus 2 µM nifedipine (black trace), and the nifedipine-sensitive current (gray trace).

(C) Late currents from (B) are displayed on a more sensitive scale. Since TTX-sensitive I_{Na} is represented by the difference between the two traces, the major component was nifedipine-sensitive I_{Ca}.

(D) Late currents were measured at increasing times (100, 250, and 500 ms) after the depolarizing pulse (applied at time zero). Late I_{Na} was, respectively 32%, 36%, and 39% of the total current (N=4). Total late current density (at 100 ms) was 0.86% of peak I_{Na}, and late I_{Na} was 0.28% of peak, in reasonable agreement with a recent estimate (Terrenoire et al., 2013). Error bars: standard error of mean (SEM).

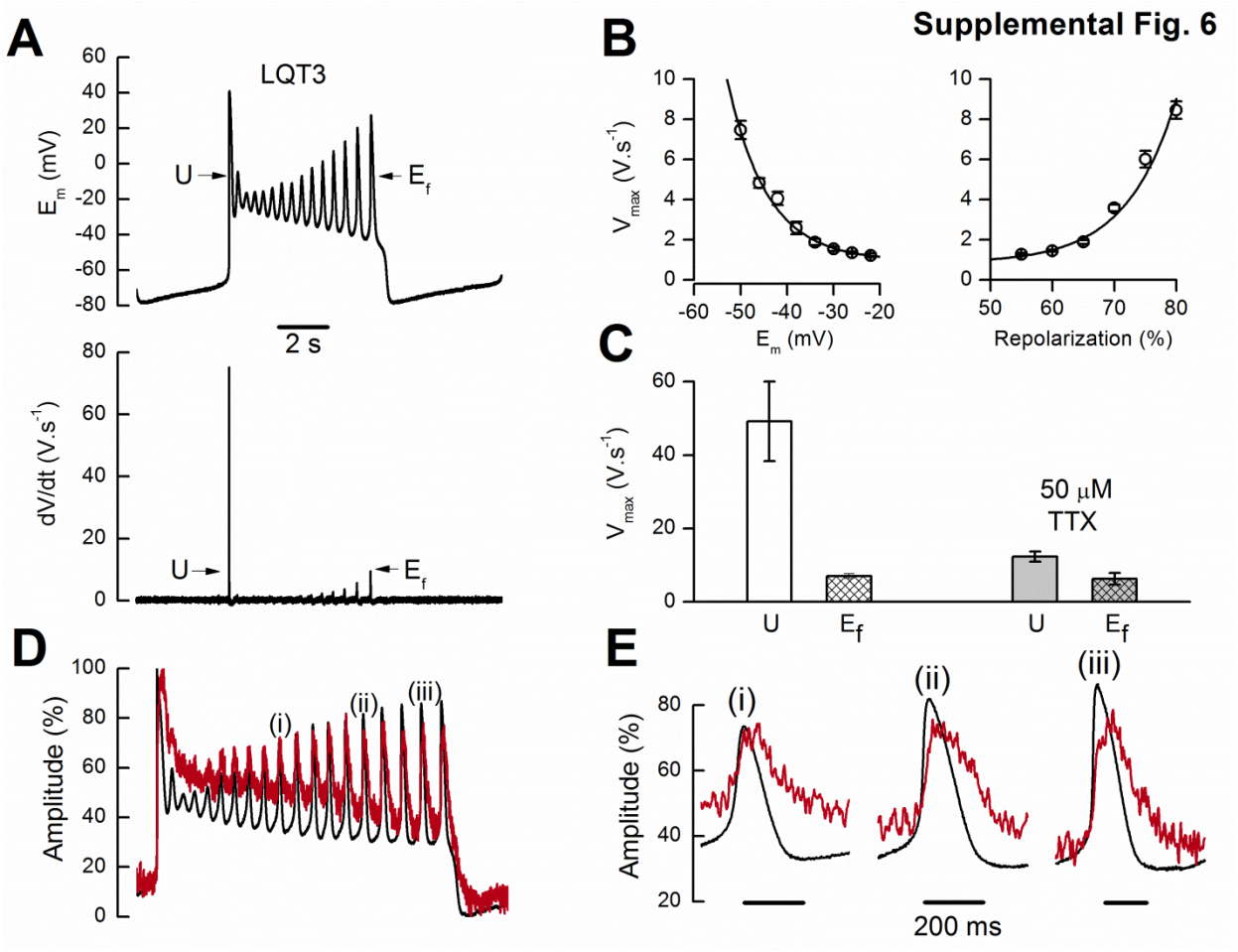
Supplemental Fig. 6
A
LQT3
U
E_f
E_m (mV)
2 s
dV/dt ($V.s^{-1}$)
B
V_{max} ($V.s^{-1}$)
E_m (mV)
Repolarization (%)
C
V_{max} ($V.s^{-1}$)
50 μM
TTX
D
Amplitude (%)
(i)
(ii)
(iii)
E
200 ms

<u>Figure S6</u>. Relationships between E_m and $[Ca^{2+}]_i$ transients during EADs in LQT3 iPS-CM: related to Figure 6.

(A) LQT3 (A3) AP ($E_{m,}$ upper panel) and the calculated differential of voltage (lower panel). The labels U and E_f refer to the initial AP upstroke and final EAD closest to terminal repolarization, respectively.

(B) Left: For many EADs, peak dV/dt (V_{max}) in EADs is plotted against the take-off potential binned at 4-mV intervals (N = 14 LQT3 (A3) microclusters). Right: V_{max} data from the left panel plotted against the binned degree of repolarization (%) at the take-off potential. In both panels, fits are a single exponential. Though V_{max} increased with repolarization voltage, it remained <10 V/s.

(C) Histogram showing mean V_{max} for the AP upstroke (U) and for E_f, compared before and during exposure to 50 µM TTX (N = 6 LQT3 (A3) microclusters). V_{max} in EADs was TTX-insensitive and similar in magnitude to AP upstrokes recorded in TTX, indicating that most Na^+ channels were closed during the EADs. Error bars: standard error of mean (SEM).

(D) Overlay of a representative AP and $[Ca^{2+}]_i$ transient normalized to maximum and minimum levels during the sweep. Every EAD evoked a $[Ca^{2+}]_i$ transient.

(E) The numbered EADs shown in (D) can be observed to decay ahead of the associated $[Ca^{2+}]_i$ transients, implying that the I_{Ca} was terminated by Ca^{2+}-dependent inactivation due to Ca^{2+} ions released from the SR into the restricted subsarcolemmal space (Brette et al., 2004; Grandi et al., 2010; Trafford et al., 1995; Weber et al., 2002).

Supplemental Fig. 7

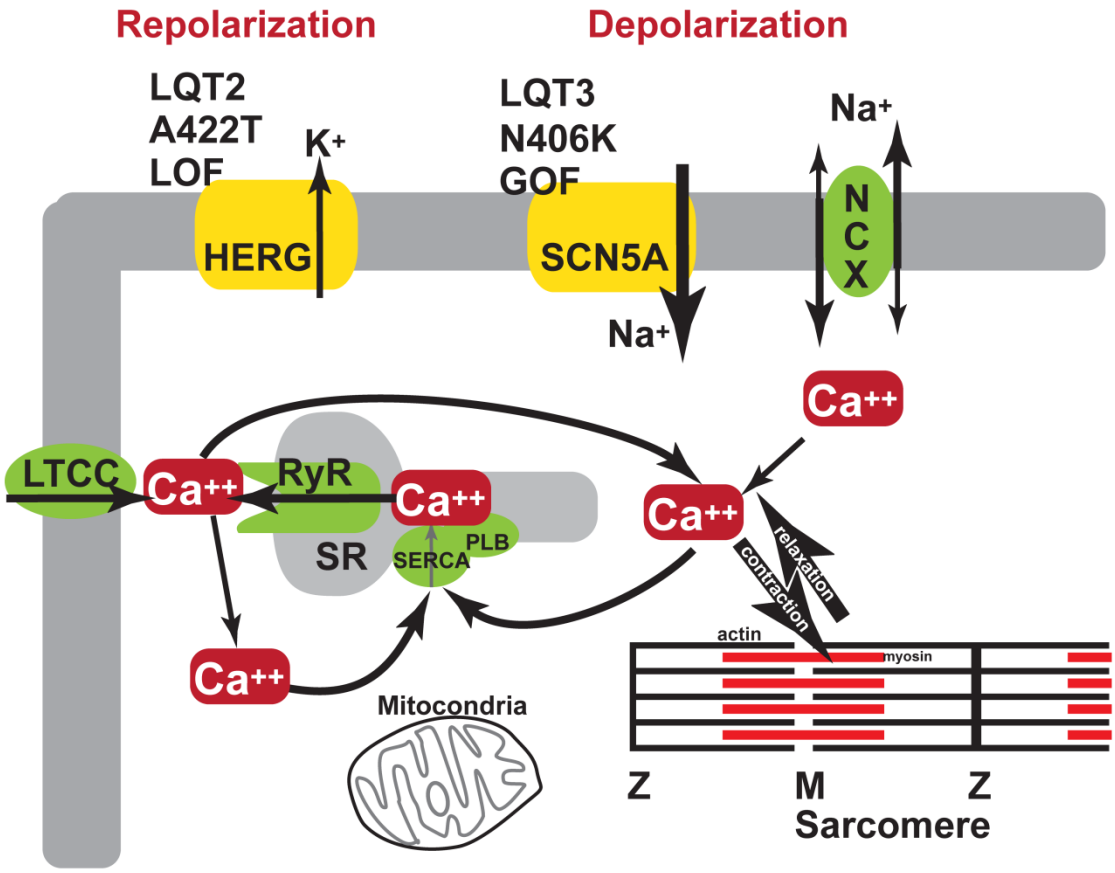

<u>Figure S7</u>. Conceptual model of the effects of LQTS mutations in cardiomyocytes: related to Discussion. The labeled ion channels and transporters are shown embedded in the sarcolemmal membrane (gray). During depolarizations, L-type Ca^{2+} channels (LTCC), admit Ca^{2+} into the subsarcolemmal space. This Ca^{2+} influx triggers SR Ca^{2+} release channels, the ryanodine receptor (RyR) channels, to open, releasing Ca^{2+} from the SR lumen and leading to a global increase in intracellular [Ca^{2+}] ($[Ca^{2+}]_i$ transient). The $[Ca^{2+}]_i$ transient inactivates LTCC, and activates myofibrillar motion and cell contractions, and also trans-sarcolemmal Ca^{2+} transport via bidirectional Na^+-Ca^{2+} exchange (NCX). In NCX, three Na^+ ions are transferred across the membrane in the opposite direction as a single Ca^{2+} ion; therefore, a net Na^+ inward current accompanies Ca^{2+} efflux (and vice versa, depending on the membrane potential). The LQT2 A422T mutation imparts loss of function (LOF) on the HERG channel, and therefore compromises repolarization. Insufficient repolarization permits Ca^{2+}-dependent inward NCX current to prolong the depolarization (i.e., the AP), which facilitates further Ca^{2+} influx (via LTCC), thereby causing EADs that may underlie cardiac arrhythmias. In LQT3, N406K is a gain-of-function (GOF) mutation in *SCN5A*, leading to an abnormally large, mistimed, net Na^+ influx. When NCX reverses (because of membrane potential) and admits Ca^{2+} into the cytosol instead of transporting it out of the cell, the amplitude of the subsequent $[Ca^{2+}]_i$ transient increases, prolonging the depolarizing phase via increased Ca^{2+} efflux once the membrane potential reverts NCX back to its normal state. This results, ultimately, in an electrophysiological phenotype equivalent to that of LQT2.

Table S1. Pooled action potential parameters measured from control, LQT2 and LQT3 iPS-CM clusters: related to Figure 6.

Genotype	V_{max} (V/s)	MDP (mV)	OSP (mV)	APD_{90} (ms)
Control (N=21)	65.9 ± 8.7	−73.2 ± 0.8	+39.5 ± 1.9	588.5 ± 53.5
LQT2 (N=13)	31.6 ± 5.0	−79.0 ± 2.3	+41.6 ± 3.3	4627.0 ± 926.3***
LQT3 (N= 31)	43.6 ± 4.9	−83.2 ± 1.1	+33.9 ± 1.3	6153.6 ± 1437.6***

Table S1. Parameters: V_{max}, maximum depolarization rate of AP upstroke; MDP, maximal (most negative) diastolic E_m between APs; OSP, overshoot potential or action potential peak voltage; APD_{90}, action potential duration at 90% repolarization. Pooled values from whole-cell and perforated patch clamp were derived by averaging over multiple successive APs in each microcluster. *** = $p < 0.001$ relative to control.

Supplemental Movie Commentary

Videomicrograph of an unpatched large microcluster of LQT3 iPS-CMs beating spontaneously. Superimposed on the video is a software-generated contrast-edge motion detector, the signal from which (generated by LabView processing of the AVI file) is shown in the graph at the bottom. The beating rhythm is bimodal, with twitches originating at a low frequency but consisting of many higher-frequency EADs. Recording at 30 fps. Playback at 60 fps.

Supplemental Experimental Procedures

Reprogramming Fibroblasts into iPS Cells

Cell lines established using dermal fibroblasts sampled from the LQTS patients and control subjects are deposited at the Coriell Institute for Medical Research (http://ccr.coriell.org/). The reprorammed iPS cells were maintained under feeder-free conditions on Matrigel in mTeSR1 medium (Stemcell Technologies, 05850). Differentiation was performed by modifying reported protocols (Bajpai et al., 2008; Kita-Matsuo et al., 2009; Nakamura et al., 2009; Zhang et al., 2012). The LQT mutations were confirmed and retroviral reprogramming generated multiple iPS cell lines (Figure S1C). Two iPS lines for each genotype were studied further. These cells demonstrated silencing of exogenous reprogramming genes, pluripotent marker expression (Figure S1B), a normal karyotype (Figure S1D), and the capacity to differentiate into all three embryonic germ layers in vitro and in vivo (Figure S2A and S2C). For immunocytochemistry, primary antibodies were: OCT3/4 (1:100) (Santa Cruz, SC-5279), SOX2 (1:100) (R&D Systems, MAB2018), NANOG (1:100) (R&D systems, AF1997), and TRA-1-81 (1:100) (Chemicon, MAB4381). Secondary antibodies were Alexa fluor 488 goat anti-mouse IgG (1:500) (Invitrogen, A-11001), Alexa fluor 488 goat anti-rabbit IgG (1:500) (Invitrogen, A11008), Alexa fluor 555 goat anti-mouse IgG (1:500) (Invitrogen, A21422), and Alexa fluor 488 goat anti-mouse IgM (1:500) (Invitrogen, A21042). Nuclei were counterstained with 1 mg/ml Hoechst 33342 (Invitrogen, H3570).

Differentiation of iPS cells into patient-specific cardiomyocytes

To characterize LQTS mutations functionally, the two selected clones of iPS cells were differentiated into cardiomyocytes (iPS-CMs) using a directed differentiation method. The iPS-CMs exhibited spontaneous beating and, after fixation, stained brightly for biomarkers characteristic of cardiac cells: cardiac troponin T (cTNT), myosin heavy chain (MHC), atrial and ventricular myosin light chains (MLC2a, MLC2v), and connexin 43 (CX43) (Figure S2D). Primary antibodies were as follows: cTNT (1:200) (Thermo Scientific, MS-295-P), MHC (1:50) (Millipore, 05-833), MLC2a (1:200) (ProteinTech Group Inc. 10906-1-AP), MLC2v (1:200) (Synaptic Systems, 311 011), CX43 (1:400) (Santa Cruz, SC-101660,), α-fetoprotein (AFP) (1:100) (R&D Systems, MAB1368), α-smooth muscle actin (αSMA) (pre-diluted) (DAKO, 1A4), and β-III-tubulin (βIIIT) (1:200) (Chemicon, CB412). The secondary antibodies were as listed above. Again, the $Na_V1.5$-N406K and $K_v11.1$-A422T gene mutations were reconfirmed by cDNA sequencing, and we verified that control iPS-CM lacked these mutations and also expressed appropriate biomarkers.

RT-PCR analysis for detecting exogenous genes

Dermal fibroblasts, P10 undifferentiated iPS cells, and human embryonic stem cells (H9 line) were harvested in Trizol (Invitrogen) for RNA isolation. Total RNA from each sample was reverse-transcribed with Superscript III (Invitrogen, 18080044) to synthesize complementary DNA (cDNA). The primers for amplifying exogenous genes of *SOX2, OCT3/4, KLF4*, and *c-MYC* in iPS cells were used as previously described (Takahashi et al., 2007). PCR conditions were as follows: DNA denaturation at 94°C for 60 s, 36 cycles at 94°C for 10 s, 55°C–62°C for 10 s, and 72°C for 30 s, followed by a final

extension step at 72°C for 5 min. For amplifying the *SOX2* exogenous gene, 5% dimethyl sulfoxide (DMSO, Sigma) was added to enhance the reaction.

Sequencing of genomic and complementary DNA

Genomic DNA was extracted from dermal fibroblasts and undifferentiated iPS cells. The primers employed for detecting the LQT2 mutations (*KCNH2* 1264G>A, K_V11.1-A422T) in genomic DNA were as described (Splawski et al., 1998). The primers for detecting the LQT3 mutation (*SCN5A* 1218C>A, Na_V1.5-N406K) in genomic DNA were: 5′-CCTCAGGTCCGCAGGGAAGAT-3′ (sense) and 5′GCTTTTCCTTCTCCTCGGTCT-3′ (antisense). PCR conditions for these primers were DNA denaturation at 95°C for 5 min, 35 cycles of 94°C for 1 min, 58°C for 2 min, and 72°C for 2 min, followed by a final extension step at 72°C for 15 min. In addition, cDNA was synthesized from differentiated iPS-CMs. *KCNH2* primers for cDNA were: 5′-CCACCAGTGACCGTGAGAT-3’ (sense) and 5′-GGCGTAGCCACACTCGGTAG-3’ (antisense). The primers for the *SCN5A* mutation in cDNA were: 5’-GGGCCTTTCTTGCACTCTTC-3’ (sense) and 5’-ACATCTCCAAGGAGCTACGG-3’ (antisense). PCR conditions were: DNA denaturation at 95°C for 5 min, 40 cycles of 94°C for 30 s, 55°C for 30 s, and 72°C for 1 min, followed by a final extension step at 72°C for 7 min.

Immunocytochemistry

The iPS cells and iPS-CMs were fixed with 4% paraformaldehyde (PFA) in PBS for 15 min at 4°C and subsequently blocked with 2% skim milk in PBS containing 0.1% Triton X-100 for 1 hr at room temperature. Primary antibodies used are listed above.

Bisulfite genomic sequencing for DNA methylation assay

Bisulfite treatment was performed using the Epitect Bisulfite Kit (Qiagen, 59110) and amplified products were cloned into pCR2.1-TOPO (Invitrogen, K451022). Randomly selected clones were sequenced with the recommended M13 forward and M13 reverse primers for each gene. Primers for the *OCT3/4* promoter regions were as previously described (Yu et al., 2009).

Teratomas

After harvest by collagenase IV treatment (GIBCO, 17104019) iPS cells were resuspended in mTeSR medium containing 10 μM ROCK inhibitor. Approximately 10^6 cells were injected directly into the testes of severe combined immunodeficiency (SCID) mice (Charles River, Wilmington, MA). Eight weeks after injection, tumors were fixed with 4% PFA, and twenty histological slices were cut (randomly) around the center of each teratoma. Sliced tissue was stained with hematoxylin and eosin, and examined by eye for tissue formations by a skilled pathologist. All animal-handling procedures followed the Guide for the Care and Use of Laboratory Animals published by the US National Institutes of Health (NIH Publication No. 85-23, revised 1996) and the guidelines of University of California San Francisco Animal Care and Use Committee.

References

Bajpai, R., Lesperance, J., Kim, M., and Terskikh, A.V. (2008). Efficient propagation of single cells Accutase-dissociated human embryonic stem cells. Mol Reprod Dev *75*, 818-827.

Brette, F., Salle, L., and Orchard, C.H. (2004). Differential modulation of L-type Ca2+ current by SR Ca2+ release at the T-tubules and surface membrane of rat ventricular myocytes. Circ Res *95*, e1-7.

Grandi, E., Morotti, S., Ginsburg, K.S., Severi, S., and Bers, D.M. (2010). Interplay of voltage and Ca-dependent inactivation of L-type Ca current. Prog Biophys Mol Biol *103*, 44-50.

Kita-Matsuo, H., Barcova, M., Prigozhina, N., Salomonis, N., Wei, K., Jacot, J.G., Nelson, B., Spiering, S., Haverslag, R., Kim, C*., et al.* (2009). Lentiviral vectors and protocols for creation of stable hESC lines for fluorescent tracking and drug resistance selection of cardiomyocytes. PLoS One *4*, e5046.

Nakamura, K., Salomonis, N., Tomoda, K., Yamanaka, S., and Conklin, B.R. (2009). G(i)-coupled GPCR signaling controls the formation and organization of human pluripotent colonies. PLoS One *4*, e7780.

Splawski, I., Shen, J., Timothy, K.W., Vincent, G.M., Lehmann, M.H., and Keating, M.T. (1998). Genomic structure of three long QT syndrome genes: KVLQT1, HERG, and KCNE1. Genomics *51*, 86-97.

Takahashi, K., Tanabe, K., Ohnuki, M., Narita, M., Ichisaka, T., Tomoda, K., and Yamanaka, S. (2007). Induction of pluripotent stem cells from adult human fibroblasts by defined factors. Cell *131*, 861-872.

Terrenoire, C., Wang, K., Chan Tung, K.W., Chung, W.K., Pass, R.H., Lu, J.T., Jean, J.C., Omari, A., Sampson, K.J., Kotton, D.N*., et al.* (2013). Induced pluripotent stem cells used to reveal drug actions in a long QT syndrome family with complex genetics. J Gen Physiol *141*, 61-72.

Trafford, A.W., Diaz, M.E., O'Neill, S.C., and Eisner, D.A. (1995). Comparison of subsarcolemmal and bulk calcium concentration during spontaneous calcium release in rat ventricular myocytes. J Physiol *488 (Pt 3)*, 577-586.

Weber, C.R., Piacentino, V., 3rd, Ginsburg, K.S., Houser, S.R., and Bers, D.M. (2002). Na(+)-Ca(2+) exchange current and submembrane [Ca(2+)] during the cardiac action potential. Circ Res *90*, 182-189.

Yu, J., Hu, K., Smuga-Otto, K., Tian, S., Stewart, R., Slukvin, II, and Thomson, J.A. (2009). Human induced pluripotent stem cells free of vector and transgene sequences. Science *324*, 797-801.

Zhang, J., Klos, M., Wilson, G.F., Herman, A.M., Lian, X., Raval, K.K., Barron, M.R., Hou, L., Soerens, A.G., Yu, J*., et al.* (2012). Extracellular matrix promotes highly efficient cardiac differentiation of human pluripotent stem cells: the matrix sandwich method. Circ Res *111*, 1125-1136.